International Journal of Material Forming (2021) 14:917–928
https://doi.org/10.1007/s12289-020-01607-3

ORIGINAL RESEARCH

Numerical modeling of mechanical properties of UAM reinforced aluminum hat sections for automotive applications

Hyunchul Ahn[1,2] · M. Bryant Gingerich[3] · Ryan Hahnlen[4] · Marcelo J. Dapino[3] · Farhang Pourboghrat[2,3]

Received: 20 July 2020 / Accepted: 4 December 2020 / Published online: 8 January 2021

Abstract
Structural lightweighting is a key initiative in the automotive sector due to regulatory, customer, and powertrain demands. This research focuses on reinforcing aluminum sheet metal in strategic locations using ultrasonic additive manufacturing (UAM), as guided through an iterative optimization and simulation process. Among the three models used, the most successful is the multi-step model (MSM) which simulates the forming of tailored blanks and the unloading processes to accurately map the hardening and the residual stress in hat and reinforcement sections. The MSM shows that approximately 65% of the mass can be saved by replacing a large gauged sheet metal hat section with a discretely reinforced hat section. Further increases in specific energy absorption (SEA) and additional mass savings can be expected when utilizing higher specific strength and specific stiffness materials for reinforcement such as titanium alloys, composites, or ceramic materials, all of which have been demonstrated with UAM.

Keywords Ultrasonic additive manufacturing (UAM) · Tailored-welded blank (TWB) · Specific energy absorption (SEA) · Multi-step model (MSM) · Topology optimization

Introduction

Most contemporary automotive structures are constructed from formed sheet metal blanks. Processed through industrial scale rolling mills, the blanks for these parts are typically homogenous in thickness. With single thickness blanks, the minimum gauge size is determined by the largest load required to be carried by the end use part. Any regions that do not experience similarly high loads while maintaining the same thickness result in inefficient use of material and unnecessary mass. Tailor-rolled blank (TRB) and tailor-welded blank (TWB) processes can introduce variations in blank thickness in key locations, allowing for lightweighting through down gauging most of the part while maintaining necessary strength or stiffness in critical regions due to increased material thickness. However, these thickness changes are typically limited to one or two regions for a given blank. As such, the spatial resolution of thickness tailoring in current automotive components is very coarse, a typical example being a door inner frame with a thicker material located at the hinge attachment region, Fig. 1.

The coarse spatial resolution of the current tailored blank technology is a result of the cost associated with processing two different child blanks and joining them in a separate process prior to the forming process. Using ultrasonic additive manufacturing (UAM) [1], this research investigates the benefit of having arbitrarily fine spatial resolution to vary blank thickness as dictated by topology optimization. The general process for this method is as follows:

1. Starting with a prescribed minimum thickness blank, define a reinforcement volume up to the desired maximum thickness of the optimized blank.

✉ Hyunchul Ahn
hahn@kitech.re.kr

✉ Farhang Pourboghrat
pourboghrat.2@osu.edu

[1] Advanced Textile R&D Department, Korea Institute of Industrial Technology, Ansan-si, Gyeonggi- do 15588, Republic of Korea

[2] Department of Integrated Systems Engineering, The Ohio State University, Columbus, OH 43210, USA

[3] Department of Mechanical and Aerospace Engineering, The Ohio State University, Columbus, OH 43210, USA

[4] Honda R&D Americas, LLC, Raymond, OH 43067, USA

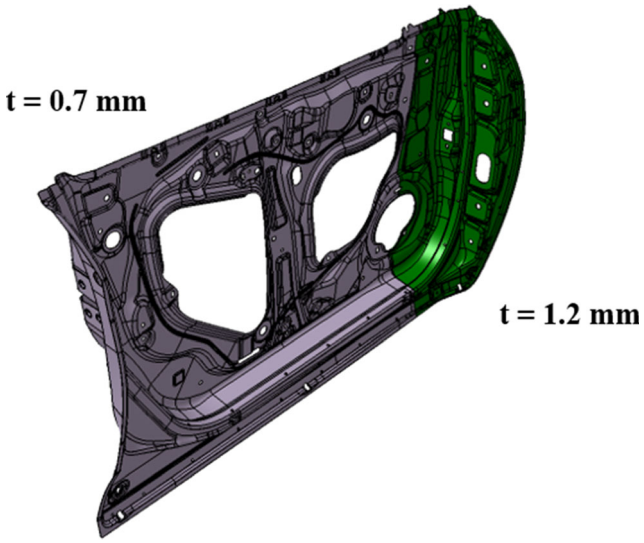

Fig. 1 TWB example component

2. Optimize the thickness and geometry of the reinforcement of a formed component for a prescribed loading condition.
3. Determine corresponding reinforcement location on the developed blank of the component.
4. Add material to the minimum thickness blank to develop the thickness-optimized regions using UAM.
5. Form the resulting component using the desired forming process.

Examples of lightweighting applications to which this concept applies include local reinforcement of bolt locations, local anti-buckling design features, and critical load path reinforcement for strength and stiffness governed designs. In these cases, the lightweighting comes from developing a minimum thickness blank and adding material where it is required by design function as opposed to maintaining a larger minimum thickness governed by a maximum local load condition.

UAM is a solid-state metal additive manufacturing process based on ultrasonic metal welding [1], Fig. 2. In the UAM process, a metal workpiece is joined to a metal baseplate using a rolling sonotrode that vibrates at high frequency in the direction perpendicular to the rolling direction. The sonotrode applies a normal load to the metal workpiece, in this case a metal foil, while the ultrasonic transducers at both sides generate oscillatory motion at approximately 20 kHz. The normal force and ultrasonic vibration deform microscopic surface asperities, breaking up and dispersing surface oxides on the workpiece and baseplate resulting in clean metal-to-metal contact and metallic bonding, as described by Graff [2].

Current UAM systems are integrated in traditional CNC milling machines, combining additive and subtractive process and enabling spatial resolution of reinforcement placement limited only by the CNC machine accuracy. This enables the addition of aluminum reinforcement to an aluminum blank, acting as a baseplate, in arbitrary shapes, locations, and thicknesses. Where tailor welded blanks require a least three processes before forming (blanking at least two child blanks and joining them), a UAM processed blank only requires blanking and the reinforcing process prior to forming while adding design flexibility.

There are other methodologies and processes that could be used to create a reinforced sheet metal blank, including discretely welding a metal patch or using other metal additive processes. While welding smaller reinforcement patches onto a blank provides higher spatial resolution as compared to TWB or TRB, attaching the reinforcement is accomplished via discrete resistance spot welds (RSW) or a continuous weld about the patch perimeter via metal-inert gas (MIG), laser, or other similar form of welding. With the joining area between the patch and blank comprising a small fraction of the overall faying surface, these methods provide a weaker method of reinforcement, necessitating either more welds, a larger reinforcement, a thicker reinforcement, or combination of all three

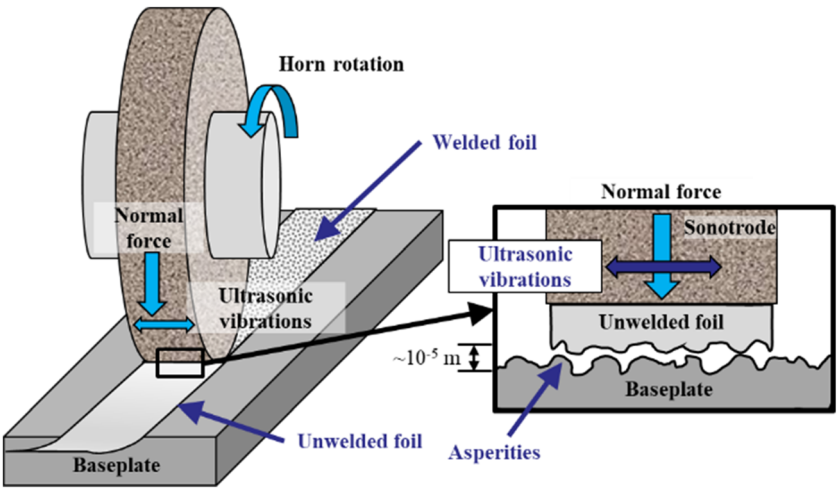

Fig. 2 Schematic diagram of the UAM process

to create a structure with equivalent properties to a UAM-reinforced blank. In contrast, UAM provides a continuous and gapless joining area over the entire faying surface [3] between the reinforcement and base metal, allowing for greater load transfer and a more efficient structure. Further, creating a metal patch would require additional tooling and fixtures for part blanking, placing, and welding, thereby increasing the process cost and complexity.

Using a different AM process avoids the issue discussed above, however, many metal AM processes such as Powder Bed Fusion (PBF) or Direct Energy Deposition (DED) require melting of the added material as well as a portion of the base material [4]. These processes not only require a controlled atmosphere and alter the microstructure of the base metal but preclude the use of dissimilar metal reinforcement or reinforcing blank materials without altering the bulk microstructure. Being a solid-state process, UAM can create metal components out of a wide variety of similar and dissimilar materials while leaving the bulk material microstructure largely unchanged. Dissimilar metal combinations made via UAM include Ti/Al composites studed by Hopkins et al. [3], Fe/Ta composites [5] and Al/steel joints [6] demonstrated by Sridharan et al., and Al/Cu composites investigated by Troug [7]. Gordon and Norfolk [8] and Hehr et al. [9] demonstrated dissimilar material combinations including non-metallic materials by constructing and characterizing UAM composites with an Al matrix and embedded Al/Al_2O_3 fiber MMC elements. Guo et al. characterized UAM composites with an Al matrix combined with carbon fiber reinforced polymers components [10].

Reinforcing the blank with dissimilar materials provides further potential for lightweighting of the formed component. In the case of specific stiffness, defined by elastic modulus over density, aluminum and steel alloys have roughly equivalent values for tensile loading, approximately 25 MN-m/kg [11]. For specific strength under tensile loading, defined by the tensile yield strength of the material divided by its density, aluminum and steel alloys again occupy similar spaces with maximum value of approximately 200 kN-m/kg.

In considering specific strength and specific stiffness, aluminum alloys have a slight advantage over steel alloys in compression and bending load cases which enable some lightweighting potential via material substitution for certain automobile components. Likewise, manufacturing constraints, such as minimum wall thickness in castings, may further favor lightweight aluminum designs that hold an advantage over steel. However, there are materials that vastly exceed both the specific strength and specific stiffness of aluminum and steel alloys for all the basic loading cases such as titanium alloys, composites, and ceramics. This material potential for lightweighting allows for significant weight reduction for current components while maintaining loading and deflection design criteria. Unfortunately, the manufacturing methods and costs associated with these materials often make direct material substitution impractical or impossible.

Cost constraints can be controlled if the high-performance materials are only used in critical load paths as determined through topology optimization. Using optimization methods combined with UAM to create reinforced blanks, this research realizes significant increases in specific performance for hat sections made of aluminum and reinforced with additional high strength aluminum alloy.

Along with experimental investigation, numerical simulation is used as a major method for problem solving in research and industrial applications due to its efficiency. Finite Element Method (FEM) analysis can be executed in either an implicit or explicit manner. In this study, the numerical analysis is accomplished using the explicit FEM simulation. One of the most important factors for sheet metal forming analysis is the material model and the stress-strain relationship, specifically the plastic deformation behavior where the deformation is relatively large and has a great influence on the simulation accuracy. For highly anisotropic materials, to accommodate for the evolution of anisotropy as a function of plastic deformation, evolutionary yield functions were developed recently by Zamiri and Pourboghrat [12], and Park et al. [13]. Springback, referring to the elastic (and sometimes elastic-plastic) recovery of metals after the forming process, has a significant influence on the geometry of the final part. Li et al. reviewed the springback simulation and studied the choice of numerical parameters such as the number of through-thickness integration points for shell-beam type elements, curvature-thickness ratios, and with-thickness ratios [14]. Moon et al. investigated the effect of tool temperature on the springback of aluminum sheet [15]. Yoon et al. predicted the springback of sheet metal forming using the hybrid membrane/shell method for reducing the computational time of finite element analyses for sheet forming with good agreement with experiments [16]. Pourboghrat et al. calculated springback of anisotropic sheet metals using a hybrid membrane/shell method, and showed that compared with a full shell model, there will be more than half of computational time saving for similar accuracy [17]. Gomes et al. investigated springback in high strength anisotropic steels [18].

In this study, for efficient sheet metal forming analysis, a simple algorithm was selected among various forming analysis theories. The chosen numerical model utilizes shell elements, the isotropic von Mises yield criterion with isotropic hardening, and a ductile damage model. In addition to forming induced strains, the multi-step model includes stamping and unloading processes. The springback analysis is typically conducted via implicit methods for accuracy, however in this study, the springback phenomenon was implemented through the explicit analysis in order to account for the entire loading/unloading history of the resulting structures.

Optimization for a three-point bending load case was performed using LS-TaSC. As shown in Fig. 3, the optimization is set up by defining a base structure and loading case in an FEA model and adding a reinforcement optimization volume consisting of a similar or dissimilar material to define the allowable reinforcement region. The optimization is set up to allocate elements of variable thicknesses within the optimization volume in order to homogenize the internal energy of each element throughout the loading case. Elements that have higher internal energy with respect to their neighboring elements have their thickness increased, while elements that have lower internal energy than their neighboring elements have their thickness decreased. Once the thicknesses of the elements in the optimization volume have been defined, the simulation is run again followed by a subsequent analysis of the elements' internal energy. This process continues iteratively until the shape of the volume converges, prescribing the optimum geometry, or a preset number of iterations is reached. The total amount of reinforcement is limited by a mass constraint on the optimization volume (i.e., 10% or 30% of the total mass of the defined optimization volume), and the geometry can be further constrained by enforcing minimum and maximum thickness to the reinforcement volume.

Hat section optimization and construction

Geometry

The geometry chosen for this study is a closed section consisting of a formed hat section and a flat plate. The hat section and plate are joined along the flange regions of the hat to create a section representative of typical structures in automotive applications. Reinforcement is attached to the inside surface of the hat.

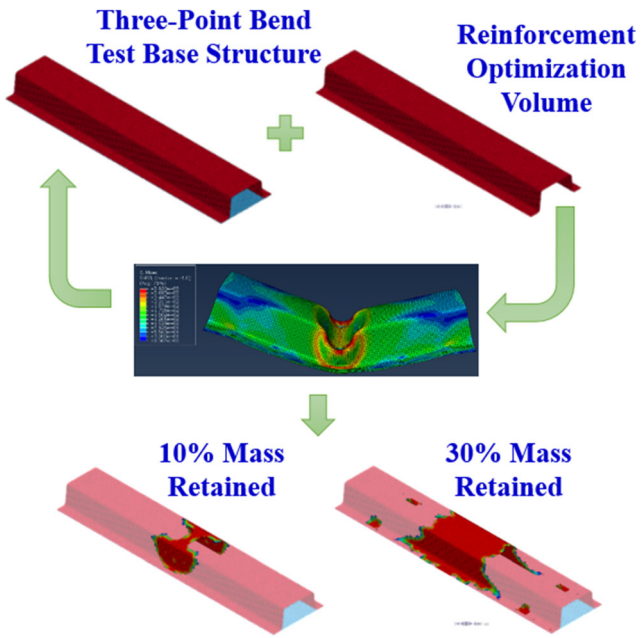

Fig. 3 Graphical representation of the process used to optimize structural reinforcement

Table 1 Mechanical properties of Investigated materials

	Al 6021	Al 6061 H18
Young's modulus (GPa)	69.0	62.6
Yield Strength (MPa)	131.0	194.0
Ductile damage properties		
Fracture strain	0.56	0.3
Stress triaxiality (η)	0.33	0.33
Strain rate ($\dot{\bar{\varepsilon}}^{pl}$)	0.1	0.005

Materials

For this study, both hats and plates are made from 1.0 mm thick Al 6021-T4 alloy. This is an alloy representative of those used for making outer panels and inner structures of automotive closures, e.g., hoods/bonnets and doors. Reinforcement consists of 0.15 mm thick Al 6061-H18 tape applied repeatedly to achieve the desired thickness. Young's modulus and yield strength of each material are determined by tensile tests based on the ASTM E8 standard. Based on tensile test results, it is assumed that both materials are isotropic with isotropic hardening property. To model the post-uniform elongation behavior of both Al alloys, the ductile damage and failure model is adopted as Eq. (1) and (2). This is a phenomenological model for predicting the onset of damage, and assumes that the equivalent plastic strain is a function of stress triaxiality (η) and strain rate [19, 20]. A displacement-based linear model is used to account for the evolution of damage. Experimentally determined mechanical properties for all materials are provided in Table 1.

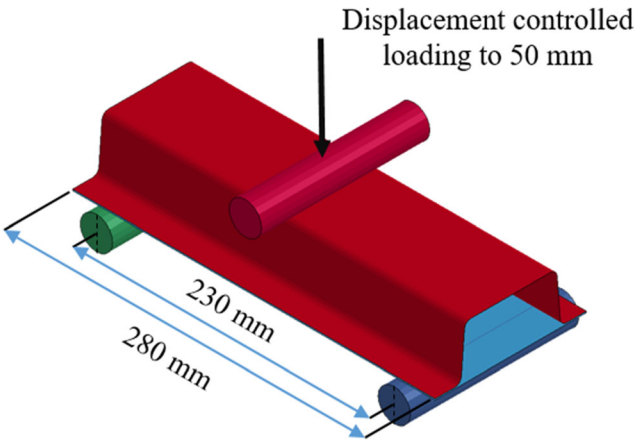

Fig. 4 Three-point bend loading case

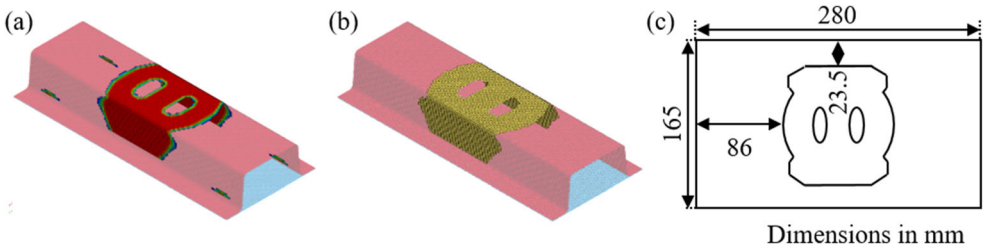

Fig. 5 Comparison of the (**a**) optimized reinforcement geometry, (**b**) generalized reinforcement geometry and (**c**) location of the generalized reinforcement patch on the developed blank for three-point bend specimens

$$\bar{\varepsilon}_D^{pl}\left(\eta, \dot{\bar{\varepsilon}}^{pl}\right) \tag{1}$$

$$\omega_D = \int \frac{d\bar{\varepsilon}^{pl}}{\bar{\varepsilon}_D^{pl}\left(\eta, \dot{\bar{\varepsilon}}^{pl}\right)} = 1, \quad \Delta\omega_D = \frac{\Delta\bar{\varepsilon}^{pl}}{\bar{\varepsilon}_D^{pl}\left(\eta, \dot{\bar{\varepsilon}}^{pl}\right)} \geq 0 \tag{2}$$

Where $\eta = -p/q$, p is the pressure, q is the Mises equivalent stress, and $\dot{\bar{\varepsilon}}^{pl}$ is the equivalent plastic strain rate. ω_D is a state variable that increases monotonically with plastic deformation.

Reinforcement optimization

The reinforcement optimization volume was applied only to the hats of the closed sections. Further, the flange area of the hat sections was excluded from the optimization volume and the reinforcement was restricted to 30% of the defined volume's mass with a maximum thickness of 1.0 mm. A three-point bend loading case is used for optimization, simulation, and experimental verification, as shown in Fig. 4. This three-point bending structure consists of a reinforced hat discretely joined to a plate via RSW. Optimizations for the three-point bend loading condition converged within 30 iterations.

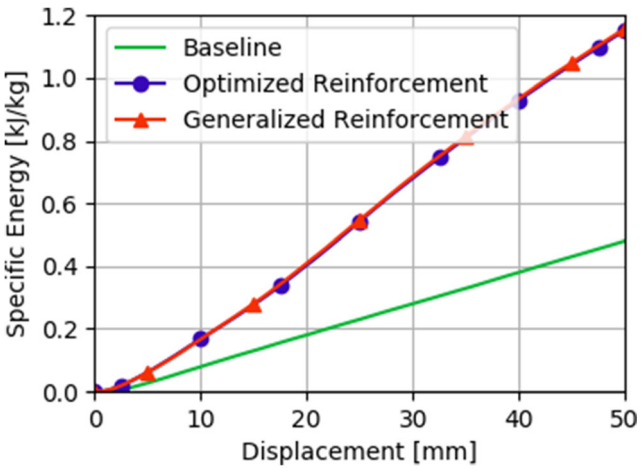

Fig. 6 Comparison of SEA versus displacement simulations for optimized and generalized reinforcement for three-point bend loading

After the optimized geometry was calculated, it was further modified to generalize the reinforcement shape. While subtractive CNC processes are available within the UAM system to make the exact duplication of the optimized structures possible, speed and ease of manufacturing is a key concern. A comparison between the optimized and generalized geometries are shown in Fig. 5 a) and b). To verify similar performance between the generalized and optimized geometries, the respective specific energy absorption (SEA) versus displacement plots were compared in Fig. 6.

Hat construction

Based upon the generalized geometry for the three-point bend reinforcement, a flat geometry is designed such that UAM can be utilized to apply the reinforcement on a flat blank, which is then formed into its final shape. This developed reinforced blank is shown in Fig. 5 c). The blank is formed into a hat shape using an aluminum die and a rubber punch with a 3-D printed surface to engage the reinforcement geometry during forming.

The developed blank consists of a 1.0 mm thick Al 6021-T4 blank reinforced with Al 6061-H18 foils up to a thickness of 1.0 mm. The reinforcement has a constant thickness except for where a 45° end mill is used to taper the edges. Once formed, the hat is joined to a 1.0 mm thick Al 6021-T4 plate via 12 RSW's. A formed three-point bend hat section prior to welding is shown in Fig. 7.

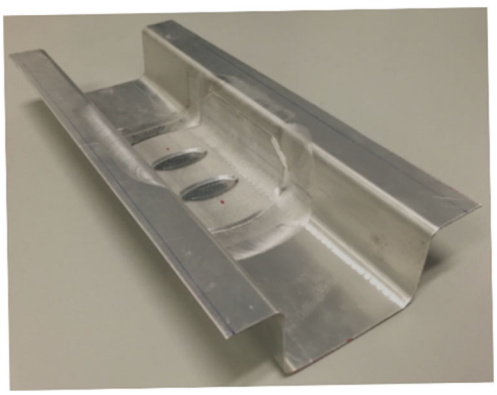

Fig. 7 Completed three-point bend reinforced hat

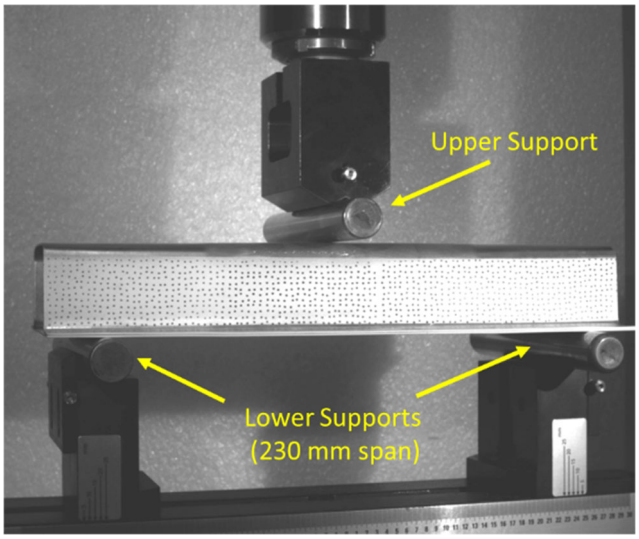

Fig. 8 Three-point bend test setup

Experimental analysis and simulation

Three point bend experiment

Three-point bend testing is performed on the three-point bend hat structures described in the previous section. The test equipment used is an MTS C43.504 load frame fitted with MTS three-point bend fixtures. During the tests, load and stroke are recorded by the machine's 50 kN load cell and crosshead leadscrew position. In addition, a digital image correlation (DIC) system is used to record the strain field progression on the side of the three-point bend samples. To accommodate the width of the three-point-bend structures, long, 19 mm diameter rollers are used for the three supports. Pictured in Fig. 8, the upper roller is placed in the middle of the sample and the lower rollers are placed 230 mm apart. The tests are completed using a crosshead rate of 5 mm/min and a sampling rate of 10 Hz.

Three point bend simulation

In order to verify the mechanical performance, the reinforced hat structures are simulated from the initial forming process through mechanical loading. For efficient analysis, the analytical model is constructed based on rigid dies and shell models, and the friction coefficient is assumed to be 0.1 on all surfaces. In the three-point bend test, this assumption is acceptable because its deformation behavior is a simple tensile-compressive deformation. To model the individual spot welds, a 3-D solid model is applied at each prescribed weld location, and each part is assumed to have perfect bonding with the hat section and plate. In the case of the blank and the reinforcement, perfect bonding is assumed for the efficiency of analysis. This is justified because no delamination of the reinforcement is observed during forming or the experiments. The material properties used in the numerical analysis are described in Table 1. In addition, elastic and hardening properties are assumed to be isotropic and ductile damage parameters introduced in Section 2 are applied. The structure of the analytical model and procedure are as shown in Fig. 9. Since the structure is based on a sheet forming process, the change in material properties through work hardening is large, and it is the aim of this study to predict it efficiently. Therefore, the work hardening behavior was realized through three different simulation methods in addition to a simple no-hardening model

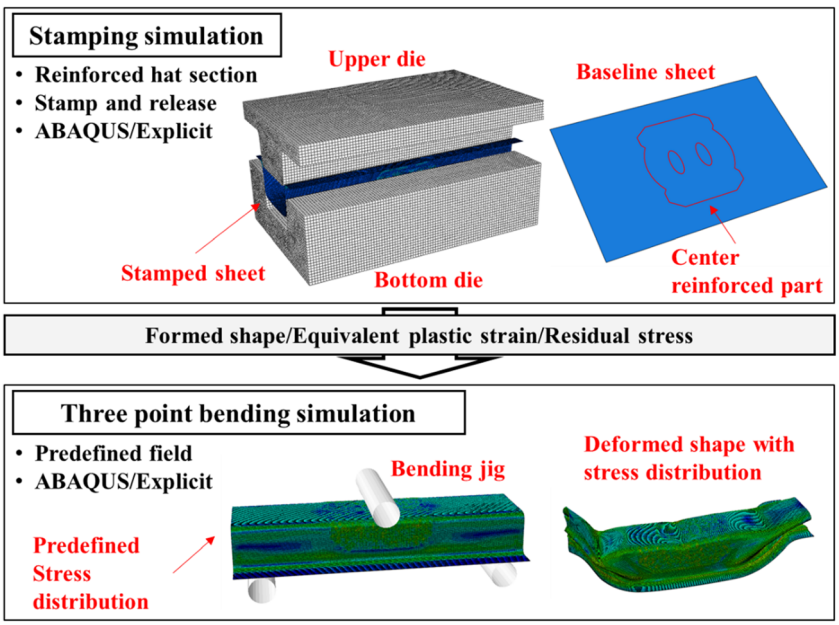

Fig. 9 Schematic of the multi-step simulation method

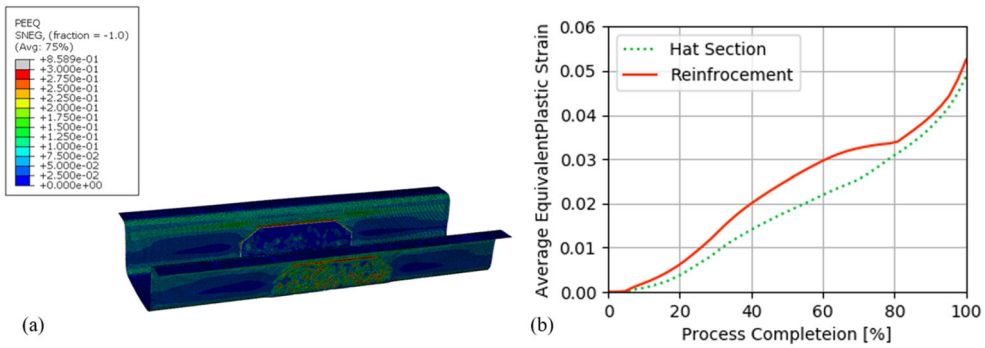

Fig. 10 **a** Equivalent plastic strain distribution after stamping simulation and **b** averaged equivalent plastic strain of hat section and reinforcement part

(NHM) with elastic-perfectly plastic material models. The simulations of the stamping process were designed for efficient analysis of the mechanical behavior and loading history, considering work hardening and residual stress effects. In order to realize the hardening effect, the analysis was conducted using three different approaches. Each analysis model has a difference in stamping shape and residual stress input variables, which affects the accuracy and efficiency of the analysis model. In addition, the computation time and model production cost also differ according to the detail of the variables, and the detailed differences between the three models are as follows.

The first model, the mean value model (MVM), uses uniform hardening by applying the equivalent plastic strain (PEEQ) from the stamping process to the bending analysis. In this study, the hardening effect is implemented through the PEEQ value for the baseline and reinforced hat structures. The PEEQ value is used as a constant and is obtained by averaging over the part as shown in Fig. 10. This method has the advantage that the analysis can be performed quickly after mapping the plastic strains from the forming process.

The second method, the sectional hardening model (SHM), applies the PEEQ to each part divided by deformation distributions and boundary conditions. In this study, 11 separate sections were used to describe the reinforced part, as shown in Fig. 11 (a), boundary conditions, and the deformation conditions. The hat section was separated into 8 representative sections. The wall and corners were sectioned into different parts, with each part being sectioned again according to the contact condition with the reinforcement. Regarding the reinforcement, all sections of the part are in contact with the hat section because it is on the inside of the hat section. However,

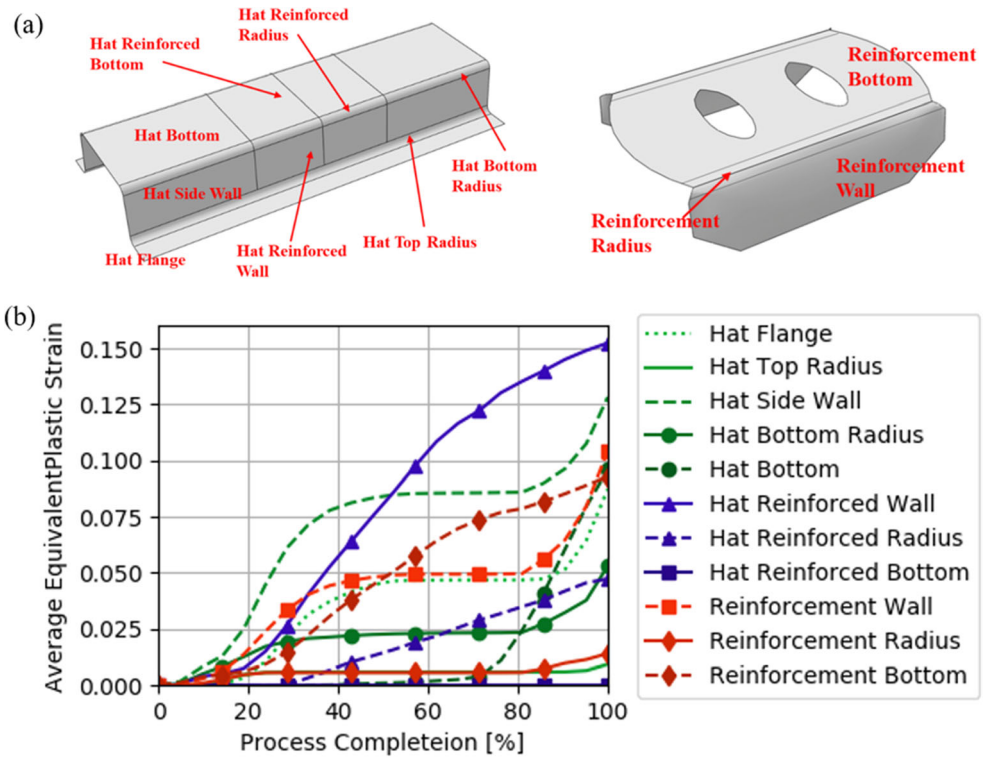

Fig. 11 **a** Eleven sections of the reinforced hat and **b** averaged equivalent plastic strain of each section

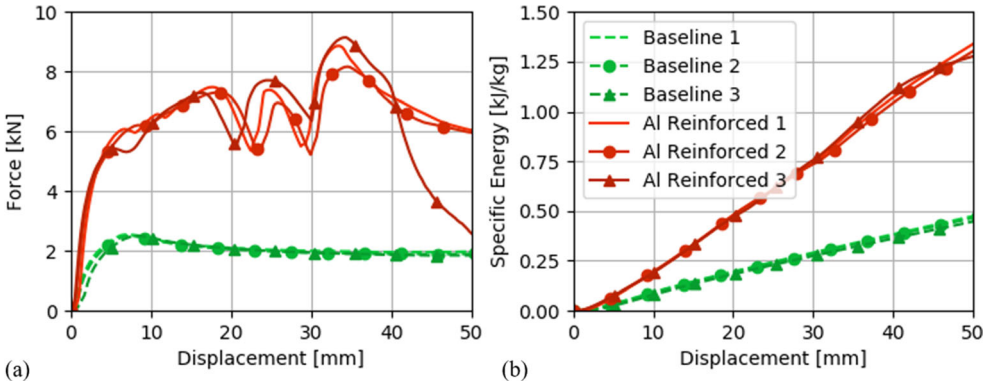

Fig. 12 Three-point bend force vs. displacement and SEA vs. displacement for baseline and Al reinforced samples

its deformation behavior is different according to the contact region, so it was separated into 3 distinct sections according to the curved and non-curved areas as shown in Fig. 11 (a).

The last model is the multi-step model (MSM), which considers the overall residual stress and PEEQ of the stamping process and applies them in the bending analysis. The SHM can explain the work hardening effect on the reinforced hat section. However, its mechanical behavior cannot be explained because of the residual stress and deformation accumulated during forming. Even though SHM can consider the deformation behavior according to the forming process, it does not account for the residual stress of the hat section and the reinforcement part. There is residual stress due to different material properties and hardening behavior, which affect the mechanical behavior of the structure. This method can provide the most accurate analysis but requires a longer computational time compared with other methods. In the MSM method, the stamping process and the unloading processes were included to obtain the residual stress and deformation like the actual forming process. As shown in Fig. 10 (a), there is significant residual stress remaining in the part after the forming and unloading process. In order to simulate the actual process, unloading by die movement rather than springback analysis was carried out. This is advantageous since unloading follows the stamping process by simply reversing the punch direction. Also, the stability of the analysis is higher than the typical method in which the springback simulation is performed separately using an implicit code. Finally, the analytical results of three numerical models were compared to the experimental results for validation of the models.

Results and discussion

Experimental results

Because the reinforced hats are compared to non-reinforced baseline hats, their overall mass is increased along with their resulting strength and stiffness. To normalize the results, all structures are compared by their SEA. The SEA is calculated by first determining the total energy absorbed during the three-point bend test through integrating the force-displacement curve. The energy absorption is then divided by the test sample's total mass to give the SEA. This provides a measure of lightweighting potential for the reinforced structure. Weight reduction would be realized by designing a structure's reinforcement such that energy absorbed is equal to the non-reinforced baseline structure. By utilizing the

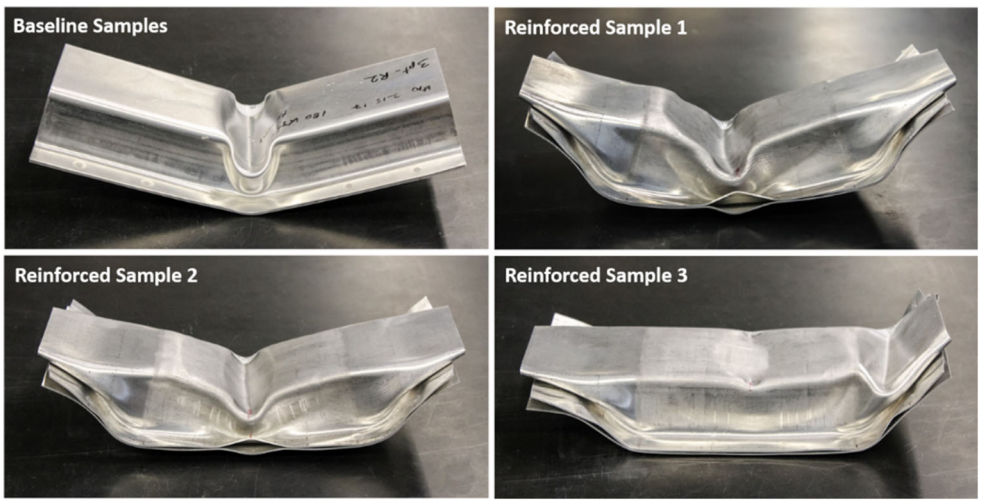

Fig. 13 Photos of tested hat-plate samples, showing representative failure modes for baseline and Al reinforced cases

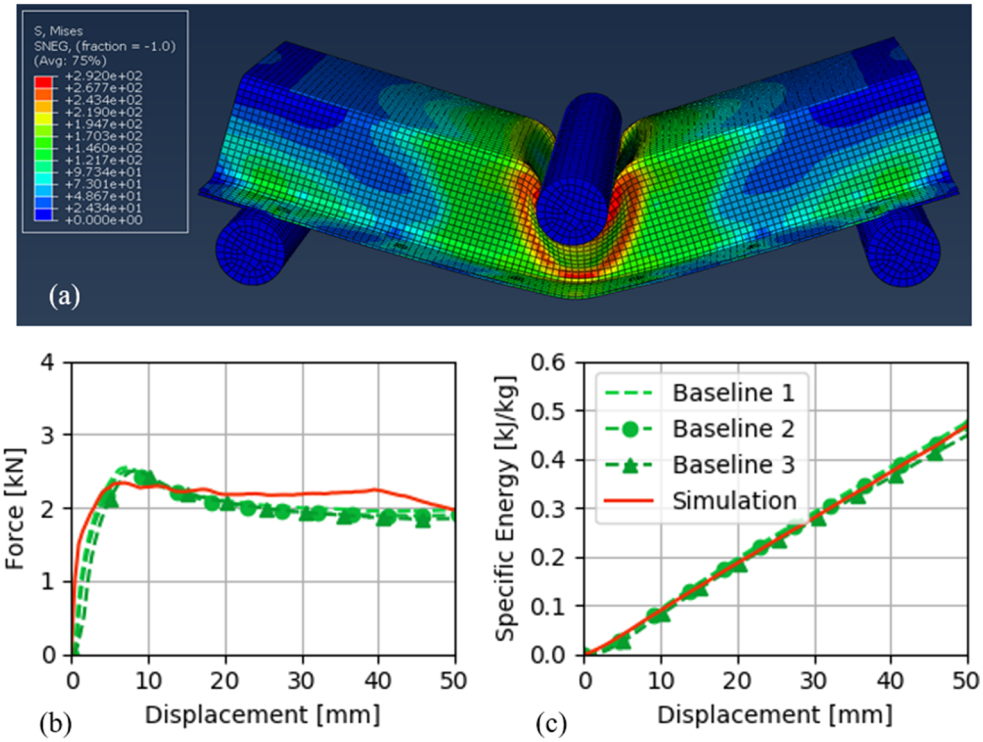

Fig. 14 Baseline model simulation result. **a** Deformed shape at 50 mm displacement with stress distribution, **b** force-displacement plot, and **c** SEA-displacement plot

reinforcement to increase the overall absorbed energy, the blank thickness of the reinforced structure can be minimized, therefore saving mass.

Three-point bend tests on the reinforced hat-plate structures show dramatic SEA improvement over the baseline hat-plate structures. The average SEA of Al reinforced samples at a displacement of 50 mm is 1.317 kJ/kg, a 187% increase over the baseline samples which have an average SEA of 0.459 kJ/kg at 50 mm.

Each of the Al reinforced samples exhibits multi-stage bending and collapse during testing. For these samples, the reinforcement in the center resisted bending, forcing deformation in regions interfacing the lower roller supports. This results in the first two peaks in the force vs. displacement curves seen in Fig. 12. The final peak is due to bending in the reinforced central region for Al reinforced samples 1 and 2 and due to bending at one end for Al reinforced sample 3. Figure 13 shows pictures of the baseline and reinforced samples after testing.

Simulation results

The numerical analysis and the experimental results of the baseline model are shown in Fig. 14. In the case of the baseline component, deformation of each section from the stamping process is uniform, and the effect of deformation of both wall surfaces, which is the main region carrying load in three-point bending, is not large enough to exhibit significant hardening, as shown in Fig. 14 (a). For the studied materials, it is experimentally and numerically determined that work hardening is very large in tensile loads, but not a significant effect in the current forming process due to the relatively small plastic strain.

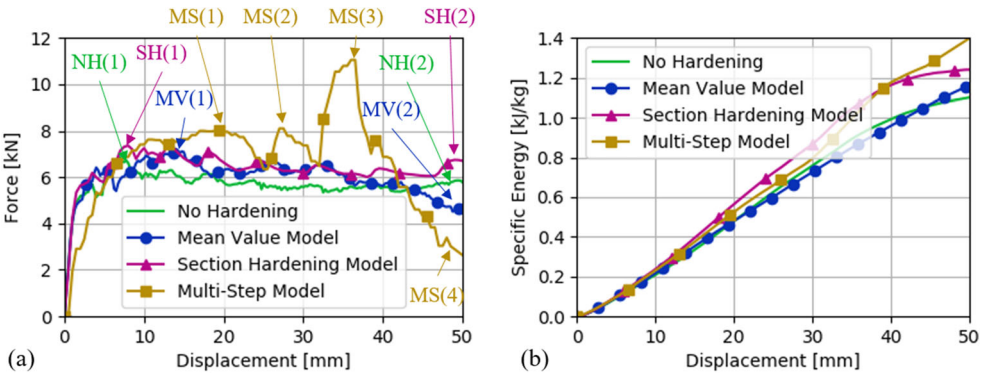

Fig. 15 Simulation results of reinforce hat section models. **a** Force-displacement result of each model and **b** specific energy absorption of each model. The indicated points represent peak loads for each model

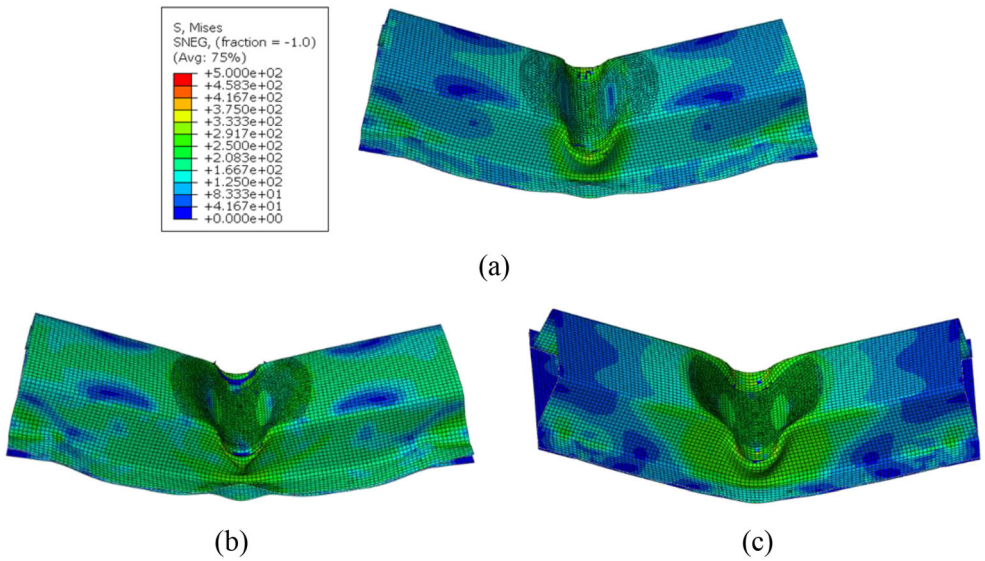

Fig. 16 Simulation result of NHM, MVM, and SHM. **a** the final shape of the NHM at the NH(2) point, **b** the final shape of the MVM at the MV(2) point, **c** the final shape of the SHM at the SH(2) point

As shown in Fig. 12, the experimental force-displacement behavior has multiple peaks because of the change in properties and yielding behavior of the reinforced parts. This behavior is a phenomenon that does not appear in the NHM because it does not include stain hardening or residual stress from forming. The multiple peaks exhibited in the experiments are due to work hardening in the hat and reinforcement during the forming process. As can be seen from the test results, the weakest region of the hat, the center, is strengthened and stiffened by the reinforcement, ultimately transmitting more load to the rest of the structure. This same effect can only be seen in the third model, which considers both the residual stress and the detailed plastic strain distribution.

For the MVM, the detailed behavior of the model is shown in Fig. 15. The stress is close to that of the NHM and still shows a significant difference with respect to the experimental result. This model also cannot explain reinforcement and hardening effect. According to the model, the peak force is slightly increased by about 3.5% as shown by points NH(1) and MV(1) in Fig. 15, however, due to hardening, the peak load point and SEA of the MVM results are slightly higher than the NHM.

The SHM has the effect of applying more work hardening to 11 discrete sections, Fig. 11, which results in a higher maximum force value than the MVM, as shown in Fig. 15. However, as shown in Fig. 16, the maximum deformation and the final deformed part show the same shape as the NHM and MVM in the middle region and do not simulate the effects of the reinforcement as shown in the experimental results. The reason for the observed difference in the deformed shape can be explained by the residual stress that prevents middle region from deforming. However, due to the hardening effect, the peak force and SEA are increased and closer to the

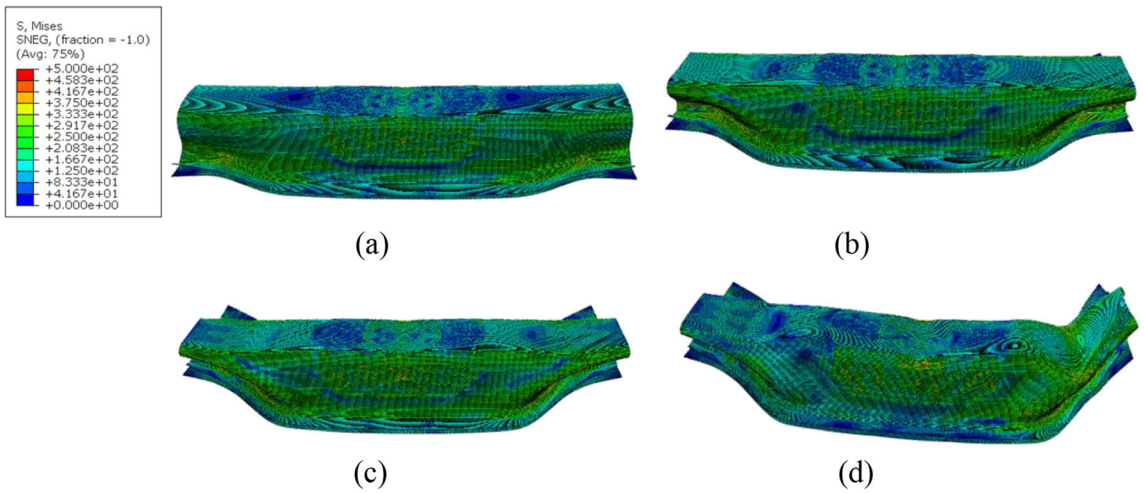

Fig. 17 Simulation result of multi-step model. **a** The first peak at the MS(1) point, **b** the second peak at the MS(2) point, and **c** the third and highest peak at the MS(3) point, and **d** deformed shape after 50 mm displacement at the MS(4) point

experimental result. Even though the multi-peak behavior is not exhibited by the SHM model, the SEA is well predicted by the hardening effect of the materials.

In the case of MSM, the results more closely correlate with the experiments, as shown in Fig. 17. The force-displacement behavior in Fig. 15 (a) differs from other models, exhibiting three peaks, as seen in the experimental data. Also like the experimental result, one side wall is deformed first as shown in Fig. 17 due to residual stress and hardening effects. This different order of deformation is due to the residual stress and work hardening from the initial step as shown in Fig. 16 (a). The deformation is not symmetric between the left and right sides due to the stamping and unloading processes. As shown in Fig. 10 (a), the residual stress and deformation are not exactly symmetric due to possible slight differences in die-part contact condition and different edge effects. As the result, plastic deformation started at the weakest point in the part leading to local stress concentration and finally asymmetric propagation throughout the formed part. Moreover, unlike a typical springback simulation, the unloading process in this method can cause asymmetric residual stress and plastic strain distribution. The non-reinforced side wall collapses in two different locations corresponding to the locations of left and right support rollers contacting the flat plate. These events are identified in the force-displacement curve as MS(1) and MS(2) in Fig. 15. As the side walls continue to deform and fold over on themselves, a third peak, MS(3), occurs corresponding to the yielding of the top of the hat under the central load roller. In the MSM, the subsequent reduction in force is due to further bending of the hat and plate above the right roller until maximum test displacement is reached. Due to this behavior, the initial peak force, maximum peak force, and SEA are higher than the other models. In fact, the MSM model shows a 199% higher SEA compared with the base model, similar to the SEA increase observed in experimental results.

Experiment and simulation comparison

The experimental and numerical result is compared and shown in Fig. 18. Overall, the MSM simulation matches the experimental force-displacement curve very well. As mentioned above, the center region of the structure exhibits less deformation compared to the baseline structure due to the reinforcement strengthening effect. Meanwhile, the primary deformation in the reinforced structure is manifested in the side walls and accurately recreated in the simulation. Both the experiment and MSM force-displacement curves show three peaks with the third peak having the peak force associated with the initiation of the top-center region deformation.

The difference between the simulated and experimental peak force is approximately 2 kN, or 20.6%, which is attributed to differences in hardening rate, imperfect contact conditions, friction, isotropic material model, etc. After the final force peak, the force drops drastically until the end of the ram displacement. This corresponds to the bending of the non-reinforced right side of the hat-plate section. This matches well with the experimental results of reinforced sample 3, showing the same deformation mechanism as in Fig. 13.

In the case of SEA, experimental and MVM simulated results for the baseline structure match very well. There is less than a 1% difference between the simulated and experimental curves. The MVM and MSM showed similar SEA output, indicating that plastic strain and work hardening of the base hat section is negligible. In the case of reinforced model, the SEA from the MSM also matches the experimental results well with less than 4% difference. This shows that MSM accurately explains the reinforced hat section behavior. The MSM is also the only model that can explain the multiple peaks in the force-displacement plot and match the characteristic deformation behavior. The model accuracy is achieved by simulating the isotropic material properties and the stamping process through the MSM simulation. In addition, the model has a

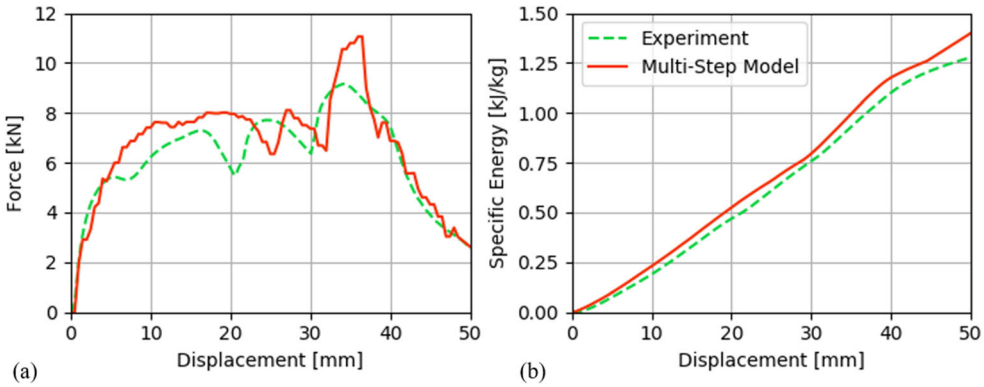

Fig. 18 Comparison between experimental and numerical results from the reinforced hat section simulation. **a** Force-displacement behavior of the reinforced model and **b** specific energy absorption of the baseline and the reinforced model

relatively simple algorithm and analysis process, which enables fast and effective computation. It is also expected that MSM can be applied to various complex structures and reinforcing materials due to its numerical stability.

Conclusions

In this study, an aluminum hat-plate structure is reinforced with high strength aluminum for the purpose of increasing the structure's SEA in three-point bend loading, ultimately leading to the ability to down-gauge from thicker, heavier structures. The reinforcement shape and thickness were determined through topology optimization and the reinforcement was applied to the aluminum blank via UAM, which enables a wide variety of dissimilar material reinforcement options.

The construction and loading of the hat section were numerically simulated using three different approaches with the objective of balancing accuracy and computational time. The best modeling strategy is MSM, which simulates the forming and the unloading processes to accurately map the hardening from plastic strain and the residual stress in the hat and reinforcement pieces. The resulting simulation accurately predicts the shape of the force-displacement curve, SEA curve, and final deformed shape of the reinforced component.

Both the experiments and simulations show an increase of 187% and 199% in SEA over the baseline. Further increases in SEA and additional mass savings are expected when utilizing higher specific strength and specific stiffness materials for reinforcement such as titanium alloys, composites, or ceramic materials, all of which have been demonstrated with UAM.

Acknowledgments The authors would like to acknowledge and thank Honda R&D Americas, LLC for the support of this research.

Compliance with ethical standards

Conflict of interest The authors declare that they have no conflict of interest.

References

1. Hahnlen R, Dapino MJ (2014) NiTi–Al interface strength in ultrasonic additive manufacturing composites. Compos Part B 59:101–108. https://doi.org/10.1016/j.compositesb.2013.10.024
2. Graff K (2005) 9 - Ultrasonic metal welding. In: Ahmed N (ed) New developments in advanced welding. Woodhead publishing, pp 241-269. https://doi.org/10.1533/9781845690892.241
3. Hopkins CD, Dapino MJ, Fernandez SA (2010) Statistical characterization of ultrasonic additive manufacturing Ti/Al composites. J Eng Mater Technol 132(4):041006-041006-041009. https://doi.org/10.1115/1.4002073
4. Haghdadi N, Laleh M, Moyle M, Primig S (2021) Additive manufacturing of steels: a review of achievements and challenges. J Mater Sci 56(1):64–107. https://doi.org/10.1007/s10853-020-05109-0
5. Sridharan N, Norfolk M, Babu SS (2016) Characterization of steel-ta dissimilar metal builds made using very high power ultrasonic additive manufacturing (VHP-UAM). Metall Mater Trans A 47(5): 2517–2528. https://doi.org/10.1007/s11661-016-3354-5
6. Sridharan N, Wolcott P, Dapino M, Babu SS (2017) Microstructure and mechanical property characterisation of aluminium–steel joints fabricated using ultrasonic additive manufacturing. Sci Technol Weld Join 22(5):373–380. https://doi.org/10.1080/13621718.2016.1249644
7. Truog AG (2012) Bond improvement of Al/cu joints created by very high power ultrasonic additive manufacturing. The Ohio State University
8. Gordon BL, Norfolk M (2015) Selective reinforcement using metal matrix composite and ultrasonic additive manufacturing. In: SAMPE 2015, Baltimore MD, May 19–20 / 2015
9. Hehr A, Wenning J, Norfolk M, Sheridan J, Newman JA, Domack M (2019) Selective reinforcement of aerospace structures using ultrasonic additive manufacturing. J Mater Eng Perform 28(2): 633–640. https://doi.org/10.1007/s11665-018-3614-1
10. Guo H, Gingerich MB, Headings LM, Hahnlen R, Dapino MJ (2019) Joining of carbon fiber and aluminum using ultrasonic additive manufacturing (UAM). Compos Struct 208:180–188. https://doi.org/10.1016/j.compstruct.2018.10.004
11. Ashby MF (2011) Chapter 5 - materials selection—the basics. In: Ashby MF (ed) Materials selection in mechanical design, Fourth edn. Butterworth-Heinemann, Oxford, pp 97–124. https://doi.org/10.1016/B978-1-85617-663-7.00005-9
12. Zamiri A, Pourboghrat F (2007) Characterization and development of an evolutionary yield function for the superconducting niobium sheet. Int J Solids Struct 44(25):8627–8647. https://doi.org/10.1016/j.ijsolstr.2007.06.025
13. Park T, Abu-Farha F, Pourboghrat F (2019) An evolutionary yield function model based on plastic work and non-associated flow rule. Metals 9(5):611
14. Li KP, Carden WP, Wagoner RH (2002) Simulation of springback. Int J Mech Sci 44(1):103–122. https://doi.org/10.1016/S0020-7403(01)00083-2
15. Moon YH, Kang SS, Cho JR, Kim TG (2003) Effect of tool temperature on the reduction of the springback of aluminum sheets. J Mater Process Technol 132(1):365–368. https://doi.org/10.1016/S0924-0136(02)00925-1
16. Yoon J-W, Pourboghrat F, Chung K, Yang D-Y (2002) Springback prediction for sheet metal forming process using a 3D hybrid membrane/shell method. Int J Mech Sci 44(10):2133–2153. https://doi.org/10.1016/S0020-7403(02)00165-0
17. Pourboghrat F, Karabin ME, Becker RC, Chung K (2000) A hybrid membrane/shell method for calculating springback of anisotropic sheet metals undergoing axisymmetric loading. Int J Plast 16(6): 677–700. https://doi.org/10.1016/S0749-6419(99)00067-4
18. Gomes C, Onipede O, Lovell M (2005) Investigation of springback in high strength anisotropic steels. J Mater Process Technol 159(1): 91–98. https://doi.org/10.1016/j.jmatprotec.2004.04.423
19. Hooputra H, Gese H, Dell H, Werner H (2004) A comprehensive failure model for crashworthiness simulation of aluminium extrusions. International Journal of Crashworthiness 9(5):449–464. https://doi.org/10.1533/ijcr.2004.0289
20. Smith M (2016) Abaqus analysis user's guide, version 2016. Simulia, Providence, RI